8-28-2019

Fabrication of micro-scale radiation shielding structures using tungsten nanoink through electrohydrodynamic inkjet printing

Hao Lyu
Iowa State University and Qingdao University of Science and Technology

Xiao Zhang
Iowa State University, xiao1@iastate.edu

Fei Liu
Iowa State University, fliu@iastate.edu

Yanhua Huang
Iowa State University, yanhuah@iastate.edu

Zhan Zhang
Iowa State University, zhan@iastate.edu

See next page for additional authors

Fabrication of micro-scale radiation shielding structures using tungsten nanoink through electrohydrodynamic inkjet printing

Abstract

Electronics components used in space and strategic missions are exposed to harsh radiation environments, which could cause operational malfunction of the system through lattice displacement or ionization effects. One potential solution is to use tungsten as radiation shielding. Tungsten is a very effective material in shielding electronic components and manufacturing gratings for x-ray imaging. However, intrinsic properties of tungsten (e.g. density, chemical/thermal inertness and hardness) post a significant challenge of fabricating the material into micro-scale and delicate structures, especially in electronic device fabrication. To address the problem, we designed a new tungsten nanoink and developed a straightforward approach to create tungsten micro-structures by 3D printing. Various microstructures down to 10 μm resolution have been patterned and fabricated by electrohydrodynamic inkjet (e-jet) printing using tungsten nanoink. By optimizing process parameters (voltage modality) and materials properties (ink formulation), the dimension and morphology of the structures can be precisely controlled. An AC-modulated voltage was employed during the e-jet printing process to make the patterns much more controllable and stable. Multi-layer tungsten lines were characterized by x-ray imaging and exhibited excellent absorption of x-ray radiation. With the same thickness, printed lines showed nearly 1/3 absorptivity of x-ray radiation of bulk tungsten, leading to significant radiation attenuation effectiveness. Tungsten nanoink is a new material used in e-jet printing that has not been reported in the literature to the best of authors' knowledge. The study establishes a new methodology of manufacturing micro-nano scale shielding components for electronic devices and rapid prototyping of gratings and collimators in radiography for medical and inspection applications. The research also provides practical guidance to fabricate high melting-point metals via nanoink and micro/nano scale 3D printing.

Keywords

radiation shielding, electrohydrodynamic inkjet printing, tungsten nanoink, x-ray imaging

Disciplines

Industrial Technology | Materials Science and Engineering | Mechanical Engineering | Nanoscience and Nanotechnology

Comments

This is a peer-reviewed, un-copyedited version of an article accepted for publication/published in *Journal of Micromechanics and Microengineering*. IOP Publishing Ltd is not responsible for any errors or omissions in this version of the manuscript or any version derived from it. The Version of Record is available online at DOI: 10.1088/1361-6439/ab3b26. Posted with permission.

Authors

Hao Lyu, Xiao Zhang, Fei Liu, Yanhua Huang, Zhan Zhang, Shan Jiang, and Hantang Qin

Fabrication of micro-scale radiation shielding structures using tungsten nanoink through electrohydrodynamic inkjet printing

Hao Lyu[1,2], Xiao Zhang[1], Fei Liu[3], Yanhua Huang[3], Zhan Zhang[4], Shan Jiang[3,5*], Hantang Qin[1,4*]

[1] Industrial and Manufacturing Systems Engineering, Iowa State University, Ames, IA 50011 USA
[2] College of Mathematics and Physics, Qingdao University of Science & Technology, Qingdao, Shandong, 266061 China
[3] Materials Science and Engineering, Iowa State University, Ames, IA 50011 USA
[4] Center for Nondestructive Evaluation, Iowa State University, Ames, IA 50011 USA
[5] Division of Materials Science & Engineering, Ames National Laboratory, Ames, IA 50011 USA

* Corresponding authors.
E-mail: sjiang1@iastate.edu, qin@iastate.edu

Received xxxxxx
Accepted for publication xxxxxx
Published xxxxxx

Abstract

Electronics components used in space and strategic missions are exposed to harsh radiation environments, which could cause operational malfunction of the system through lattice displacement or ionization effects. One potential solution is to use tungsten as radiation shielding. Tungsten is a very effective material in shielding electronic components and manufacturing gratings for X-ray imaging. However, intrinsic properties of tungsten (e.g., density, chemical/thermal inertness and hardness) post a significant challenge of fabricating the material into micro-scale and delicate structures, especially in electronic device fabrication. To address the problem, we designed a new tungsten nanoink and developed a straightforward approach to create tungsten micro-structures by 3D printing. Various microstructures down to 10 μm resolution have been patterned and fabricated by electrohydrodynamic inkjet (e-jet) printing using tungsten nanoink. By optimizing process parameters (voltage modality) and materials properties (ink formulation), the dimension and morphology of the structures can be precisely controlled. An AC-modulated voltage was employed during the e-jet printing process to make the patterns much more controllable and stable. Multi-layer tungsten lines were characterized by x-ray imaging and exhibited excellent absorption of x-ray radiation. With the same thickness, printed lines showed nearly 1/3 absorptivity of x-ray radiation of bulk tungsten, leading to significant radiation attenuation effectiveness. Tungsten nanoink is a new material used in e-jet printing that has not been reported in the literature to the best of authors' knowledge. The study establishes a new methodology of manufacturing micro-nano scale shielding components for electronic devices and rapid prototyping of gratings and collimators in radiography for medical and inspection applications. The research also provides practical guidance to fabricate high melting-point metals via nanoink and micro/nano scale 3D printing.

Keywords: radiation shielding, electrohydrodynamic inkjet printing, tungsten nanoink, x-ray imaging

1. Introduction

Electrohydrodynamic inkjet (e-jet) printing [1], a method combing electrohydrodynamics and inkjet printing, has attracted much interest recently in fabricating submicron-to-micron sized structures, including dots, lines, and films [2-4]. E-jet printing has certain advantages over the traditional lithography based techniques, such as direct-writing capabilities without the need of complex fabrication processes, extra masks, etching, or developing. In addition, e-jet printing is low-cost and highly versatile with a variety of selections of printable materials on diverse substrates [5-7]. Many metal inks were employed to generate different structures, including silver nanoparticles [8], silver nanowires [9], quantum dots [10], carbon nanotube [11] and graphenes [12]. In e-jet printing, printed patterns were deposited onto the substrate layer by layer via nano-scale control of platform movement. After solidifying, the patterns could form reliable and diverse structures as designed [13]. Based on the flexibility and precision of programmable platform movement, both regular patterns and discrete patterns could be fabricated using e-jet printing on various substrates, which has led to unique application in particular fields [14, 15], including radiation shielding patterns on electronic components. However, it is still challenging to determine the ink formulations to achieve precise and delicate printing structures.

Electronic components used in strategic and space missions are exposed to harsh radiation environments, which could cause operational malfunction of the system through lattice displacement and ionization effects. Current radiation-hardening techniques for electronics, such as using radiation-resistant materials in standard semiconductor manufacturing or adopting radiation tolerant logical designs, require specially tailored electronic design or manufacturing processes. At present, most radiation-shielding techniques require the use of heavy and thick enclosures for effective shielding, which significantly increases the structural mass of the system. One possible solution is to use precisely printed tungsten structures as radiation shielding. Tungsten, one of the most effective radiation shielding materials, has remarkable properties of density, robustness, chemical inertness, hardness, and thermal-resistivity [16, 17]. However, it is a significant challenge to manufacture designed tungsten structures due to such intrinsic properties, especially in electronic device fabrication. To overcome the challenge, we developed a new method to fabricate microstructures using with tungsten nanoparticles, which is much easier to control and manufacture compared with bulk modality [18, 19]. More importantly, nanoparticles could be formulated into nanoink with the help of appropriate additives [20], which has enabled micro/nano manufacturing based on inkjet printing and e-jet printing.

In this paper, we reported the use of e-jet printing method to fabricate micro-scale radiation shielding structures of different shapes and thicknesses using tungsten nanoink. The printed patterns showed excellent morphology and resolution, as well as good absorption of x-ray radiation. To the best of our knowledge, the tungsten nanoink used in our e-jet printing is a novel formulation that has not been reported in the literature yet. This technology paves the way for manufacturing tungsten in micro/nano scale to generate customized patterns for radiation shielding and radiography in space mission, medical, and inspection applications.

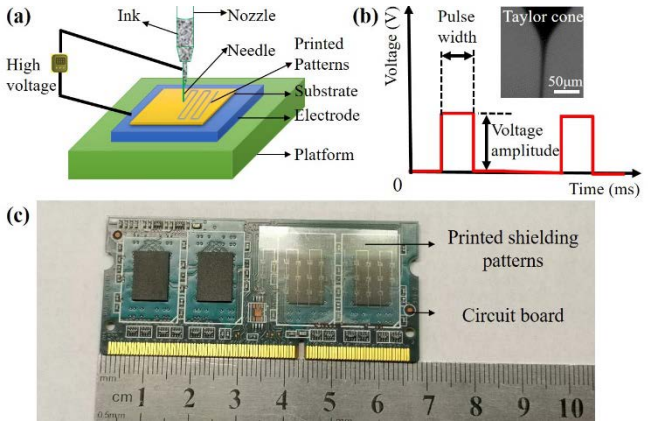

Figure 1. (a) Schematic of e-jet printing. A high voltage is applied between the needle and plate electrode. (b) Voltage modality and a machine vision of e-jet printing process. (c) A typical circuit board partially covered by printed patterns for the radiation shielding concepts.

2. Methods and Materials

2.1. E-jet printing system

To print the tungsten micro-patterns, an e-jet printing system was employed, shown in Fig.1(a). A plate electrode was set on the nano-positioning platform, which was controlled precisely by programs. A high voltage was applied between the plate electrode and needle, generating a large electric field to jet out droplets for depositions and printing. The ink was printed on the substrate attached on the plate electrode. With the moving of the platform, various patterns could be fabricated via given programs. There were several parameters affecting printing structures [21], including needle size, stand-off distance, voltage modalities, and plotting speed. By optimizing these parameters, tungsten structures with different patterns were achieved. A charge coupled device (CCD) camera, as well as a lens system, were employed to monitor the needle and printed patterns [22]. The needle with diameter ~30μm in the printing process was captured in Fig. 1(b) with optical images by CCD. With the real-time testing, we could observe the printed pattern quality, Taylor cone, droplet size, and the changes of stand-off distance. After printing, a microscope (Hirox RH-2000) was

employed to characterize the patterns and morphology of printed results. Many substrates were good candidates for e-jet printing, such as flexible films, which could be used for radiation shielding by covering on the circuit board. Fig. 1(c) showed our printed metal patterns on flexible PET film covered on the circuit board. Different substrates have different surface roughness and surface energy, which leads to different wetting profile while printing. All experiments in this study have been performed on 1.5 mm thick glass slides for calibration of the nanoink (Fisher Scientific, Waltham, MA). The printing on PET films and 36mm Kodak photo films have been conducted to demonstrate the versatility of e-jet printing and to represent common photography film that needs x-ray protection or marking (e.g., barcode) applications.

2.2. Nanoink fabrication

The raw materials used in the ink were tungsten nanoparticles with average particle size ~70nm (from US research nanomaterial, Inc), solvent Triethylene Glycol Monomethyl Ether (TGME, from Sigma-Aldrich), and Polyvinylpyrrolidone (PVP, from Sigma-Aldrich). TGME was applied as the solvent in nanoink, and PVP was used as the surfactant and thickener to facilitate the dispersing of nanoparticles in the solvent. The mass ratio of PVP to tungsten nanoparticles was 1:25, and the concentration of tungsten in TGME was 50% in mass. Because of heterogeneous-sized tungsten nanoparticles, PVPs with different molecular weights were employed as surfactants for better dispersion of tungsten nanoparticles, including 55K and 360K with a mass ratio of 1:1. In the study, fresh nanoinks with tungsten nanoparticles dispersed were prepared for printing after mixing. After the patterns were fabricated by e-jet printing, curing was not provided for most of the printed samples. Instead, the tungsten nanoink evaporates and dries on the substrate. The curing on printed parts does not influence the x-ray absorption performance because the presence of tungsten particles is the key to absorb x-ray energy under exposure to radiation. Currently, the fabrication is limited to 2D planner feature fabrication. A future research direction would be the fabrication of 3D tungsten structures, which will require the elevated temperature to increase evaporation rate and instant curing during printing.

2.3. Characterization

The commercial tungsten nanoparticles were characterized by the transmission electron microscopy (TEM, JEOL 2100), and energy dispersive spectroscopy (EDS, Oxford Aztec). In order to investigate the tungsten components contained in printed dots which were applied for radiation shielding, x-ray diffraction (XRD) with monochromatic CuKα radiation (Rigaku MiniFlex 600) was performed to identify the printed tungsten dots. The scan speed and step width were 10°/min and 0.02°, respectively..

2.4. X-ray imaging of printed patterns

The radiation characteristic of printed tungsten patterns was taken with a lab-built x-ray radiography system setup, including x-ray source, moving stage, a signal detector, control system, and analysis system, shown in Fig. 2. A 50kV, 1000μA x-ray source was employed for scanning of printed tungsten samples, where the exposure time was 6500ms to get a high-quality image. The detector with resolution 3072×3888 was used in the x-ray imaging system to obtain the x-ray transmitted data passing through the sample. Once the x-ray transmitted the sample with tungsten patterns, parts of them were absorbed, then the left arrived at the detector to form images with different grayscale values [23].

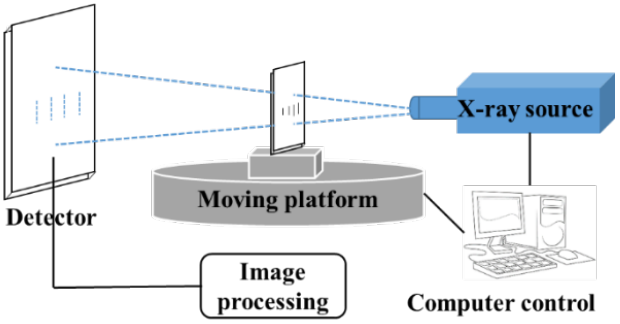

Figure 2. Schematic of the lab-built x-ray imaging system.

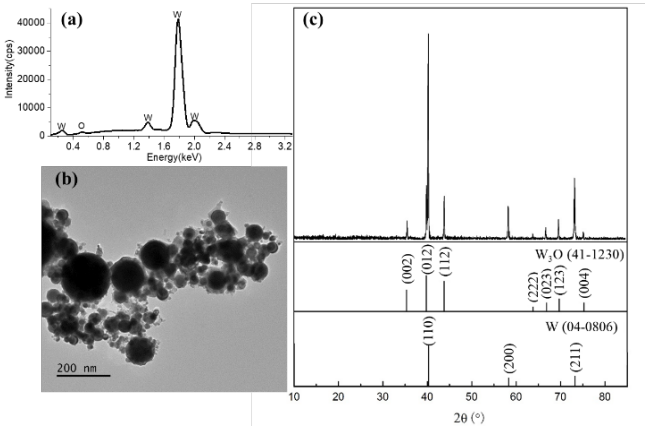

Figure 3. (a) Energy dispersive spectroscopy (EDS) and (b) transmission electron microscopy (TEM) images of tungsten nanoparticles. (c) X-ray diffraction (XRD) results of printed tungsten dots.

3. Results and discussion

The EDS results (Fig. 3(a)) indicate that the commercial nanoparticles are mainly pure tungsten. There is a small peak in 0.5keV, which suggests that oxidation exists in the nanoparticles. TEM image (Fig. 3(b)) of tungsten nanoparticles used in the study shows a polydisperse size distribution of nanoparticles. The smallest dimension of tungsten nanoparticles is about 20nm. In order to uniformly

disperse particles with such size range, two PVPs of different molecular weights (55K and 360K) were added into the tungsten nanoink to tune the rheology and stability of the ink formulation for e-jet printing. The XRD was taken to confirm the crystal structures of tungsten in the printed dots (Fig. 3(c)). The XRD peaks demonstrate that the peaks with (110) (200) (211) have high intensities. The peak values match with tungsten peaks W (04-0806), which suggests our printed tungsten has a bcc crystalline structure [20, 24]. The XRD peaks corresponding to W3O were also observed as (002) (012) (112) (222) (023) (123) (004), which further confirmed the oxidation states of tungsten nanoparticles in the nanoink. The XRD results strongly indicate that the printed tungsten is in the crystalline form, which can benefit the x-ray absorption analysis in the following part.

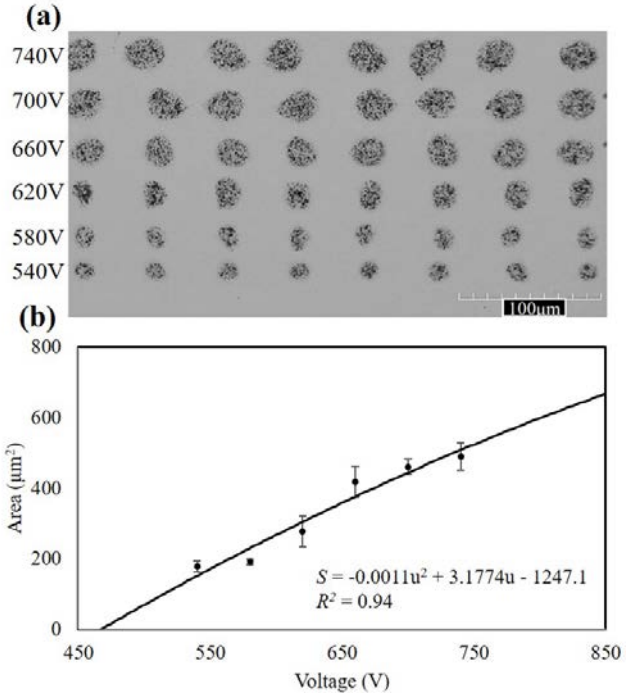

Figure 4. Printed tungsten dots with e-jet printing in different voltages. (a) optical microscope image, (b) dots area as a function of printing voltage.

The mechanism of the e-jet printing process was extremely complicated and difficult to control, due to the facts that numerous variables are coupled with each other for the printing process [21]. Presented in this work, the control of needle dimension, stand-off distance, voltage amplitude, frequency, pulse width, and plotting speed will all affect printing quality of designed patterns. Different from thermal/acoustic pressure driven inkjet printing [25], e-jet printing employes high voltages to drive the metal ink ejection, utilizing the electrical force working at Tayler cone mode, and achieve higher resolution. The changes of voltage modalities play a significant role in printed patterns morphology, especially the dimensions of the features. Fig. 4(a) shows a variation of tungsten dots printed at different printing voltages. An explicit size decrease can be observed with the reduction of voltage. With higher voltage, a large electric field force was applied to the droplet, resulting in the jet being ejected and printed onto the substrate. As the curve shown in Fig. 4(b), higher voltage yielded dots with a larger size. The trend was fit linearly with the equation $S = -0.0011u^2 + 3.1774u - 1247.1$, where S is the dotted area in micrometer^2 and u is the voltage in volt, respectively. The area of the dot is determined by the volume of the droplet in e-jet printing, which indicates the gradual changes of droplet volume with altering voltage. Under constant needle diameter and stand-off distance, the accumulation of charges in Taloy cone increases with higher voltage, generating droplets which have increased volumes and higher speeds to the substrate. Dots with a larger size can also be printed. With a ~30μm diameter needle, a small size dot with diameter ~10μm can be printed, which serves as the prior control of e-jet printing by high voltage [5].

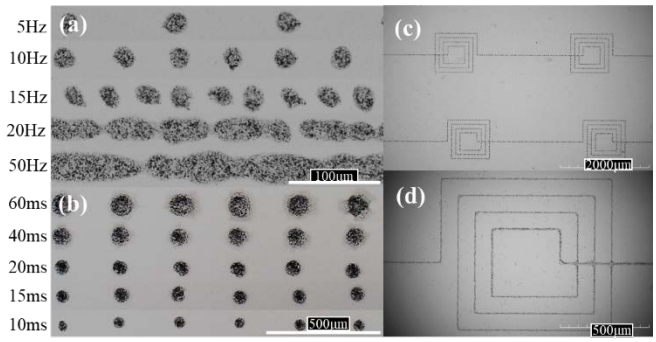

Figure 5. Optical microscope images of tungsten dots under different (a) frequencies and (b) pulse widths of high voltage; Optical microscope images of tungsten shaped lines with (c) low and (d)large magnification.

The morphology of printed patterns is closely related to the printing parameters. Instead of using direct current (DC) voltage [26] between electrode and needle which could generate many single-size dots, an amplified alternating current (AC) with variable voltage, frequency and pulse width was applied for printing in our study. Different parameters resulted in different dimensions of dots or lines. Fig. 5 shows optical images of printed tungsten dots under various frequencies and pulse widths. With high frequency, the increase in jetting frequency and spray speed leads to closer separations between two adjacent droplets and line coalescence. The distance between two contiguous dots changed from 100μm at 5Hz to 31μm at 15Hz. Further increasing the frequency produced the dots overlapping with the previous ones, which eventually resulted in coupled dots and wide lines, as shown in Fig. 5(a). The pulse width [27] is the open status of the voltage switch, which allows the supply of high voltage for printing. The length of pulse width affects the electrical field force of the ink, such that the dots can be

printed in different sizes, as shown in Fig. 5(b). The diameter of the dot decreases from 83μm to 33μm with a pulse width change from 60ms to 10ms. The dot sizes are much larger than those in Fig. 5(a), since the pulse width of Fig. 5(a) was tens of microseconds. Larger pulse width resulted in larger dot size. If the pulse width is too small, the nanoink could not come out from the needle dut to the failure of nanolink forming the fine Taylor cone. With the selected parameters, group lines in patterns of excellent fidelity were acquired, as shown in Fig.5 (c) and (d). Because of AC voltage application, the droplet can be controlled precisely, which produces good patterns even in the turning corner. The line width is about 6.5μm, shown in Fig.5 (d), much smaller than the needle diameter 30μm. It is the result of well-defined printing droplet generated by high voltage and optimized frequency [28] and speed [29]. However, there were still several imperfect dots at the cross-points of two lines since the printed nanoinks did not dry immediately. The AC voltage used in e-jet printing provided a convenient adjusting method for generating different size and morphology dots or lines. As a proof of concept, the capability of patterning is demonstrated here, which can be further optimized for future applications in manufacturing radiation shielding components for electronics.

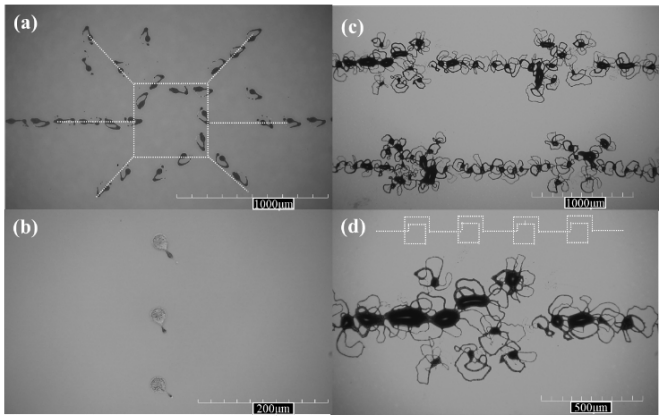

Figure 6. Optical microscope images of tungsten patterns at different conditions: (a) DC voltage and the dashed lines were the designed pattern; (b) large pulse width with AC voltage; (c) and (d) are non-fresh ink with normal and high voltage at the designed patterns as dashed lines in inset. The dashed lines denote designed printing path.

Several interesting patterns were obtained by altering printing parameters, as shown in Fig.6. Violent droplets flying behavior was observed when printing using DC voltage. For example, the patterns like tadpoles in Fig.6(a) were printed under a pre-programmed pattern shown as the dashed lines. The DC voltage was applied between the needle and electrode, and the nanoink came out consistently. We observed that due to charges in e-jetted droplets, plotting speed, and high viscosity of the ink, a disturbance was generated with the in-flight droplets. At a particular plotting speed, a small tip left behind the dot. Large pulse width with AC voltage can also lead to tips in the dots, shown in Fig.6(b). While the ink was not fresh (aged ink after several days), there were some random patterns emerging in the printing, seen in Fig. 6(c). This could be due to the particle aggregation so that the nanoink was no longer homogeneous. Some particles and solvent came from the needle non-continuously, demonstrating electrospinning behavior with a high level of uncertainty. Some narrow lines, as well as large dots, could be generated. At this condition, when a high voltage applied, the irregular patterns were observed. Enlarged images show structures similar to diffusion-limited aggregation (Fig. 6(d))[30]. When the nanoink was not uniform and ejected randomly at high voltage, such random drops and curved lines occurred.

By adjustment pulse width, oscillate frequency and spacing, diameters of printed dots were precisely controlled by adjusting the pulsed signal for excitation. Printed line width was controlled cooperating with printing head moving velocity, excitation voltage, pulse width, and oscillate frequency [33]. Once the liquid ink was charged enough by the electrical potential to overcome the surface energy, a new surface will facilitate the resulting formation of the droplet. With controlled pulse width and amplified voltage, the electron prudential energy delivered to the ink liquid were controlled; therefore, a means of controlling droplet mass results in high printing quality [34]. Simulation work on the droplet generation has been reported in e-jet printing [35]. There were several areas with a relatively large quantity of tungsten nanoink in Fig.6 (c) and (d). They were high tungsten density patterns and could play an important role in radiation shielding. Due to the complication of ink properties and interaction with electric fields, the overall mechanisms of pattern formation and line coalescence in Fig. 6 have not been fully understood yet. A future research direction would be correlated with ink formulation and droplet dynamics under the electrical fields. More details of the relationship between tungsten pattern quality and printing parameters will be further investigated.

Generally, line patterns with 50-200nm thick have been obtained with e-jet printing after multi-layer stackup [31]. For better radiation shielding application of tungsten, multi-layer lines were also required and printed layer by layer. Fig. 7 (a) showed the optical image of printed multi-layer tungsten lines, where a round trip was designed to realize layer-by-layer printing. Since the nanoink did not solidify immediately during the printing process, there were some outflows of the line, leading to several bulge formation in multi-layer lines. When the printing layers increased to 50 layers, the solvent and tungsten regions were clearly observed in the magnified optical image Fig. 7(c). The dark line represented the tungsten line as marked in the picture, while there were also some

overflowing solvents with multi-layer printing. With a 3D imaging optical system, a general 3D picture was obtained in Fig. 7(d). The thickness of the line was about 9.5μm, which resulted from the multi-layer printing.

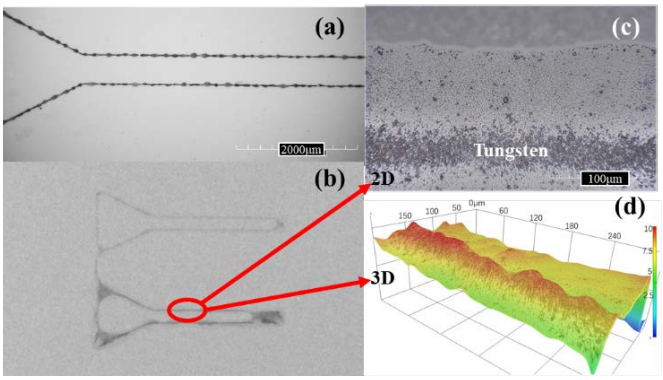

Figure 7. (a) Optical image. (b) x-ray radiography image of printed tungsten lines with 20 layers (top) and 50 layers (bottom). (c) and (d) are magnified 2D and 3D images of the 50 layers tungsten line, respectively.

Fig.7(b) showed the x-ray radiography imaging results, where the designed patterns with 20 and 50 printed layers were observed. The pictures were analyzed by Matlab and x-ray absorption was calculated. In the study, a grayscale was used to estimate the absorption of x-ray. $G=I/I_0$, where G was the grayscale of printed tungsten patterns, I and I0 was the gray value of the tungsten pattern and background of the sample, respectively. The gray value of each pixel of the patterned area and background by coordinate recognition was obtained, and the mean values of them were calculated. The calculated grayscale of the patterns in Fig. 7(b) were 0.99 and 0.97 for the top (20layer) and bottom (50layer) pattern, respectively.

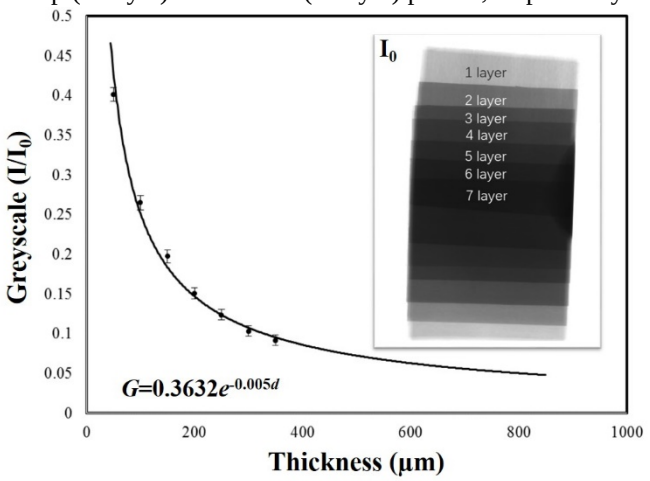

Figure 8. Grayscale of bulk tungsten sheet as a function of its thickness. The inset is an x-ray radiography image of tungsten sheets with different layers.

The x-ray radiography patterns in the image were the area filled with printed tungsten nanoparticles rather than the solvent. The absorption efficiency was affected by tungsten atoms thickness and density [32], which was determined by line layers. In order to compare the radiation shielding effect between bulk tungsten and nanoparticles, a group of standard bulk tungsten sheets (Eagle Alloys, Co.) was also used for x-ray radiation with the same system. The thickness of each sheet was 50μm, and different layers were used to adjust various thickness, shown in the inset of Fig. 8. Thus, the grayscale under different thickness tungsten sheets was calculated in Fig. 8. The change rule was matched exponentially of the equation $G=0.3632e^{-0.005d}$, where G was the calculated grayscale and d was the thickness of tungsten sheets, respectively.

Table 1. The comparison of grayscale between bulk and printed tungsten at the same thickness.

Printed Lines	Thickness Avg. / μm	Thickness Std. / μm	Grayscale Ratio I_z/I_0	Grayscale Ratio I_z/I_0	Bulk Tungsten I_z/I_0
50-Layer Print	12.5329	0.1154	0.9700	0.0031	0.4333
20-Layer Print	3.6071	0.1642	0.9913	0.0008	0.3461
1-Layer Print	0.0971	0.0269	0.9917	0.0007	N/A

The printed lines consists of tungsten nanoparticles. The presence of tungsten function as attenuation elements, but attenuation effects cannot be as good as bulk tungsten due to porosity existing in the printed structures. The study is in the range of micro/nano scale detection and x-ray intensity is evaluated by the grayscale of the resulting images. The acceleration voltage was set at 50 kV considering wide linear mass attenuation response [36] and sufficient energy for high resolution x-ray contrast at micro-scale (20 μm). In Table 1, with different printed thickness, the thickness ratios of printed tungsten comparing to bulk tungsten required to provide same x-ray shielding efficiency were calculated shows that the printed tungsten thickness increase, the shielding efficiency are close to bulk tungsten sheet. The grayscale of 20-Layer printed lines was 2.77 times smaller than bulk tungsten sheet at the same thickness, and 2.26 times smaller for 50-Layer printed lines.

The small grayscale means low transmittance and high blocking rate of an x-ray through the samples. The grayscale results indicate that the printed tungsten lines have good performance of x-ray radiation absorption, which is about 1/3 absorptivity of bulk tungsten. The grayscale is affected by both particle density and layer width. More radiation absorption and patterns of lower grayscale values can be obtained when there are more tungsten layers and higher density of tungsten on the substrate. The x-ray radiography imaging results indicate that our printed tungsten lines can indeed prevent x-ray radiation in high efficiency. However, it was still lower than bulk materials, most likely due to the packing density of tungsten nanoparticles.

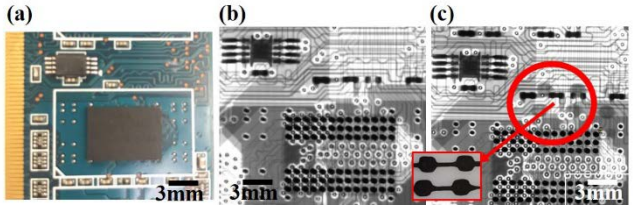

Figure 9. (a) Optical image of circuit board. (b) x-ray radiography image of the circuit board . (c) Printed capacitor and cover patterns on the circuit board under x-ray imaging

Fig. 9(a) presented the physical appearance of a circuit board from a central server. Flexible substrate (PET film) with printed tungsten ink was placed upon the circuit board to mimic two scenarios: 1) a shielding, and 2) marker in CT applications. Before the printed pattern was placed on top of the board, we can observe the x-ray image under radiation in Fig. 9(b). After the tungsten pattern was placed on it, four pad patterns could be clearly detected in Fig. 9(c). The electronic components in the circuit board (e.g., screen printed conductive lines) were covered by the tungsten components, such that shielding function can be achieved or marker (e.g., barcodes) can be detected. The micro/nano e-jet printing based strategy can create radiation shielding enclosures for electronics in a highly tailorable manner, and more importantly, can potentially enhance the radiation attenuation effectiveness with a lower structural weight.

4. Conclusion

We have successfully developed a new tungsten nanoink for e-jet printing and demonstrated different printing patterns, including dots and lines. By adjusting the printing parameters (e.g., voltage, frequency, pulse width, and ink formulation), the dimension and morphology of printed dots can be precisely controlled. The printed tungsten patterns exhibited excellent absorption of x-ray radiation under direct exposure. With the same thickness, printed lines showed about 1/3 absorptivity of x-ray radiation of bulk tungsten, exhibiting good potential applications for radiation-shielding of electronic components. This work presented a novel and convenient path to manufacturing radiation-shielding patterns with tungsten nanoparticles, which may find useful applications in the development of micro-nano electronic device for shielding protection.

Acknowledgments

The research is supported by startup accounts of Drs. Jiang and Qin at Iowa State University. Dr. Jiang would like to thank 3M for the Non-tenured Faculty Award. Dr. Lyu is a visiting scholar at Iowa State University (08/01/18-07/31/19). He is supported by the International Cooperation Program for Excellent Lectures of 2017 by Shandong Province Education Department. The support is greatly appreciated.

Declarations of interest

The patent application of the tungsten nanoink for electrohydrodynamic inkjet printing is currently under review at Office of Intellectual Property and Technology Transfer office at Iowa State University for US Patent (ISURF #04952), and at National Intellectual Property Administration (CNIPA, Chinese Patent Office). The authors declare that they have no other known competing financial interests or personal relationships that could have appeared to influence the work reported in this paper.

ORCID iDs

Dr. Hao Lyu https://orcid.org/0000-0003-3090-8653
Dr. Shan Jiang https://orcid.org/0000-0001-8119-9012
Dr. Hantang Qin https://orcid.org/0000-0003-4180-7911

References

[1] Park J U, Hardy M, Kang S J, Barton K, Adair K, Mukhopadhyay D K, Lee C Y, Strano M S, Alleyne A G, Georgiadis J G, Ferreira P M and Rogers J A 2007 High-resolution electrohydrodynamic jet printing *Nat. Mater.* **6** 782-9

[2] Prasetyo F D, Yudistira H T, Nguyen V D and Byun D 2013 Ag dot morphologies printed using electrohydrodynamic (EHD) jet printing based on a drop-on-demand (DOD) operation *J. Micromech. Microeng.* **23** 095028

[3] Jang Y, Kim J and Byun D 2013 Invisible metal-grid transparent electrode prepared by electrohydrodynamic (EHD) jet printing *J. Phys. D Appl. Phys.* **46** 155103

[4] Tekin E, Wijlaars H, Holder E, Egbe D A M and Schubert U S 2006 Film thickness dependency of the emission colors of PPE–PPVs in inkjet printed libraries *J. Mater. Chem.* **16** 4294-8

[5] Han Y and Dong J 2018 Fabrication of self-recoverable flexible and stretchable electronic devices *J. Manuf. Syst.* **48** 24-9

[6] Brossard F S F, Pecunia V, Ramsay A J, Griffiths J P, Hugues M and Sirringhaus H 2017 Inkjet-Printed Nanocavities on a Photonic Crystal Template *Adv Mater* **29** 1704425

[7] Yudistira H T, Tenggara A P, Nguyen V D, Kim T T, Prasetyo F D, Choi C G, Choi M and Byun D 2013 Fabrication of terahertz metamaterial with high refractive index using high-resolution electrohydrodynamic jet printing *Appl. Phys. Lett.* **103** 211106

[8] Lee D Y, Shin Y S, Park S E, Yu T U and Hwang J 2007 Electrohydrodynamic printing of silver nanoparticles by using a focused nanocolloid jet *Appl. Phys. Lett.***90** 081905

[9] Cui Z, Han Y, Huang Q, Dong J and Zhu Y 2018 Electrohydrodynamic printing of silver nanowires for flexible and stretchable electronics *Nanoscale* **10** 6806-11

[10]Kim B H et al 2015 High-Resolution Patterns of Quantum Dots Formed by Electrohydrodynamic Jet Printing for Light-Emitting Diodes *Nano Lett.* **15** 969-73
[11]Jeong Y J, Lee X, Bae J, Jang J, Joo S W, Lim S, Kim S H and Park C E 2016 Direct patterning of conductive carbon nanotube/polystyrene sulfonate composites via electrohydrodynamic jet printing for use in organic field-effect transistors *J. Mater. Chem. C* **4** 4912-9
[12]An B W, Kim K, Kim M, Kim S Y, Hur S H and Park J U 2015 Direct Printing of Reduced Graphene Oxide on Planar or Highly Curved Surfaces with High Resolutions Using Electrohydrodynamics *Small* **11** 2263-8
[13]Li X, Park H, Lee M H, Hwang B, Kim S H and Lim S 2018 High resolution patterning of Ag nanowire flexible transparent electrode via electrohydrodynamic jet printing of acrylic polymer-silicate nanoparticle composite overcoating layer *Org. Electron.* **62** 400-6
[14]Kim K, Kim G, Lee B R, Ji S, Kim S Y, An B W, Song M H and Park J U 2015 High-resolution electrohydrodynamic jet printing of small-molecule organic light-emitting diodes *Nanoscale* **7** 13410-5
[15]Li X, Lee G S, Park S H, Kong H, An T K and Kim S H 2018 Direct writing of silver nanowire electrodes via dragging mode electrohydrodynamic jet printing for organic thin film transistors *Org. Electron.* **62** 357-65
[16]Lee P A, Citrin P H, Eisenberger P and Kincaid B M 1981 Extended X-Ray Absorption Fine-Structure - Its Strengths and Limitations as a Structural Tool *Rev. Mod. Phys.* **53** 769-806
[17]Shemelya C M, Rivera A, Perez A T, Rocha C, Liang M, Yu X, Kief C, Alexander D, Stegeman J and Xin H J J o E M 2015 Mechanical, electromagnetic, and X-ray shielding characterization of a 3D printable tungsten–polycarbonate polymer matrix composite for space-based applications *J. Elect. Mater.* **44** 2598-607
[18]Nersisyan H H, Lee J H and Won C W 2005 A study of tungsten nanopowder formation by self-propagating high-temperature synthesis *Combust. Flame* **142** 241-8
[19]Lei H, Tang Y J, Wei J J, Li J, Li X B and Shi H L 2007 Synthesis of tungsten nanoparticles by sonoelectrochemistry *Ultrason. Sonochem.* **14** 81-3
[20]Ghosh S, Khamarui S, Saha M and De S K 2015 Fabrication of tungsten nanocrystals and silver-tungsten nanonets: a potent reductive catalyst *Rsc Adv.* **5** 38971-6
[21]Qin H T, Wei C, Dong J Y and Lee Y S 2017 Direct Printing and Electrical Characterization of Conductive Micro-Silver Tracks by Alternating Current-Pulse Modulated Electrohydrodynamic Jet Printing *J. Manuf. Sci. E-T Asme* **139** 021008
[22]Qin H T, Dong J Y and Lee Y S 2017 AC-pulse modulated electrohydrodynamic jet printing and electroless copper deposition for conductive microscale patterning on flexible insulating substrates *Robot. Cim-Int. Manuf.* **43** 179-87
[23]John M. Boonea J A S 1997 An accurate method for computer‐generating tungsten anode x‐ray spectra from 30 to 140 kV *Med. Phys.* **25** 1661-70
[24]Maillé L, C. Sant C, Le Paven-Thivet C, Legrand-Buscema C, and Garnier P 2003 Structure and morphological study of nanometer W and W_3O thin films *Thin Solid Films* **428** 237-241
[25]Sirringhaus H, Kawase T, Friend R, Shimoda T, Inbasekaran M, Wu W and Woo E J S 2000 High-resolution inkjet printing of all-polymer transistor circuits *Science* **290** 2123-6
[26]Zou W H, Yu H B, Zhou P L and Liu L Q 2019 Tip-assisted electrohydrodynamic jet printing for high-resolution microdroplet deposition *Mater. Design* **166** 107609
[27]Holtz J 1992 Pulsewidth modulation-a survey *IEEE T. Ind. Electron.***39** 410-20
[28]Mishra S, Barton K L, Alleyne A G, Ferreira P M and Rogers J A 2010 High-speed and drop-on-demand printing with a pulsed electrohydrodynamic jet *J. Micromech. Microeng.* **20** 095026
[29]Phung T H, Kim S and Kwon K-S 2017 A high speed electrohydrodynamic (EHD) jet printing method for line printing *J. Micromech. Microeng.* **27** 095003
[30]Witten Jr T and Sander L M J P r l 1981 Diffusion-limited aggregation, a kinetic critical phenomenon *Phys. Rev. Lett.* **47** 1400-3
[31]Qin H T, Cai Y, Dong J Y and Lee Y S 2017 Direct printing of capacitive touch sensors on flexible substrates by additive e-jet printing with silver nanoinks *J. Manuf. Sci. E-T Asme* **139** 031011
[32]Zhou Z, Kong B, Yu C, Shi X, Wang M, Liu W, Sun Y, Zhang Y, Yang H and Yang S J S r 2014 Tungsten oxide nanorods: an efficient nanoplatform for tumor CT imaging and photothermal therapy *Sci. Rep.* **4** 3653
[33] Nguyen, V-D and Byun D 2009 Mechanism of electrohydrodynamic printing based on ac voltage without a nozzle electrode. *Appl. Phys. Lett.* **94(17)** 173509.
[34] Zheng, G-F, Liu H-Y, Xu R, Wang X, Liu J, Wang H, and Sun D-H **2014** Alternating current electrohydrodynamic printing of microdroplets *J. Nanomater* **2014** 1-7
[35] Pan, Y, and Zeng L 2019 Simulation and Validation of Droplet Generation Process for Revealing Three Design Constraints in Electrohydrodynamic Jet Printing *Micromachines* **10.2** 94
[36]https://physics.nist.gov/PhysRefData/XrayMassCoef/ElemTab/z74.html, last accessed 08/02/2019.